DOI: http://dx.doi.org/10.15407/tpwj2019.05.01

EFFECT OF CURRENT AND ARC LENGTH ON CHARACTERISTICS OF ARC DISCHARGE IN NONCONSUMABLE ELECTRODE WELDING*

I.V. KRIVTSUN, V.F. DEMCHENKO, I.V. KRIKENT, D.V. KOVALENKO and **I.V. KOVALENKO**
E.O. Paton Electric Welding Institute of the NAS of Ukraine
11 Kazimir Malevich Str., 03150, Kyiv, Ukraine. E-mail: office@paton.kiev.ua

The method of mathematical modeling was used for investigation of the effect of current and length of atmospheric pressure argon arc with refractory (tungsten) cathode on heat, electromagnetic and gas-dynamic characteristics of arc plasma, including the characteristics of its thermal, electric and dynamic (force) impact on the anode surface. A short review of the mathematical models used for this purpose is given. The temperature fields and patterns of current flow in the arc column are illustrated with corresponding isotherms and current lines. Analysis of force effect of arc current on its column plasma is based on calculation data on distribution of magnetic pressure in arc plasma and corresponding magnetic force acting on plasma. Peculiarities of distribution of total pressure and velocity of plasma movement in the arc column are also analyzed. The calculation data are given on distribution of density of electric current and heat flow on the surface of water-cooled and evaporating anode, as well as on distribution of plasma potential along the boundary of anode layer depending on current and arc length. The concepts of effective values of anode and cathode potential drop are introduced. Proceeding from the calculation value of heat flow into the anode and experimental watt-ampere characteristic of an argon arc with a refractory cathode, the data were obtained on the value of effective efficiency of such an arc in the current range of 50–300 A for an arc of 1.5; 2 and 3 mm length. Dependence of the dimensions of current channel and zone of thermal impact of the arc on the anode on current value and arc length was determined. 26 Ref., 22 Figures.

Keywords: *arc with refractory cathode, arc current, arc length, arc plasma, arc column, anode layer, anode current density, anode heat flow, mathematical modeling*

For effective application of electric arc as the heat source in fusion welding, it is necessary to have valid information on the thermal, electric and dynamic (force) impact of arc plasma on the metal being welded, depending on the welding process and mode. In the case of nonconsumable electrode welding, when the metal being welded is the arc anode, such an impact is determined by the set of processes of energy-, mass- and electric charge transfer in the plasma column and anode region of the arc, and its characteristics depend on current, arc length and shielding gas composition. As experimental determination of the characteristics of thermal, electromagnetic and gas-dynamic processes in arc plasma, as well as its thermal, electric and dynamic impact on the weld pool surface is difficult, the objective of this work is detailed quantitative study of the above characteristics by mathematical modeling methods. We will consider as an object of investigation the axially symmetrical argon arc with a refractory cathode, the scheme of which is shown in Figure 1, in the range of currents I = 50–300 A and following values of arc length L = 1.5; 2; 3 mm. These are exactly the arc discharge parameters which are characteristic for inert-gas nonconsumable (TIG) welding.

There exists a multitude of approaches and models for numerical study of the processes energy, pulse, mass and charge transfer in the plasma of electric arc column, as well as anode processes for TIG-welding conditions [1–13]. However, in the majority of the works on complex modeling of an arc with refractory cathode rather simplified models of the anode layer are used [1–7], whereas in the works specially devoted to study of anode phenomena [8–13], insufficient attention is given to their interrelation with the processes, running in the arc column. To correctly account for this relationship, we will use a self-consistent mathematical model of the column and anode region of the arc in nonconsumable electrode welding, proposed in [14], and modified in [15].

Characteristics of arc column plasma. Let us first consider the distributed characteristics of the ther-

*Based on materials of a presentation at the IX International Conference «Mathematical modeling and information technologies in welding and related processes», September 10–14, 2018, Odessa.

mal, electromagnetic and gas-dynamic processes in the plasma of the column of an argon arc, burning between the refractory cathode and copper water-cooled (nonevaporating) anode. Figure 2 presents the results of modeling the temperature field and pattern of current flowing in the arc of length L = 2 mm for three characteristic values of arc current I = 100, 150, 200 A. Shown on the left are the current lines, which are the generatrices of the surfaces of revolution, limiting the area of the arc, within which a certain part of total current flows. The isotherms of arc plasma temperature field are given in the figures on the right. Configurations of current lines in near-electrode regions of the considered arc are indicative of its contraction in these regions: considerable near the cathode and essentially smaller near the anode. With increase of arc length, the isotherms and the current lines, accordingly, become wider that points to a reduction of the current density in longer arcs. Comparing the isotherms with the current lines, we can come to the conclusion that the dimensions of the current channel, in which 90 % of the arc current flow, are approximately two times smaller than the current-conducting region of the arc column (argon plasma becomes electrically conducting at the temperature above 4500 K).

Let us now consider the gas-dynamic characteristics of arc plasma. Electromagnetic force, resulting from interaction of the arc current with inherent magnetic field acts as the main force factor determining the gas-dynamic situation in the arc column. An actual component of this force is the vortex component of the Lorentz force [16]

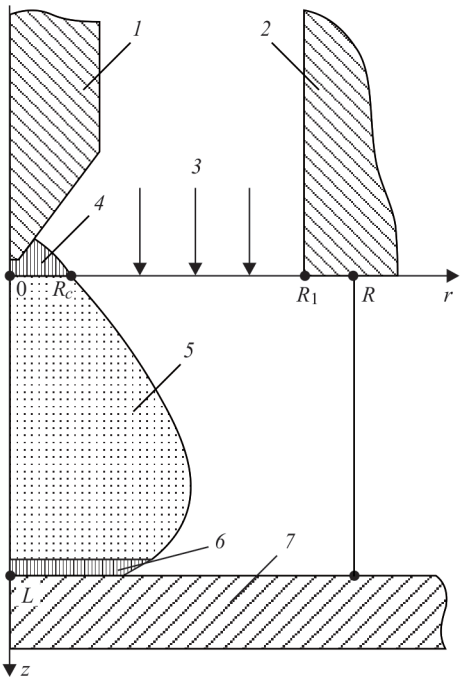

Figure 1. Scheme for calculation of the characteristics of an arc with a refractory cathode: *1* — tungsten cathode; *2* — nozzle for shielding gas feeding; *3* — shielding gas; *4* — cathode region; *5* — arc column; *6* — anode layer; *7* — anode; R_c — cathode region radius; R_1 — nozzle radius; R – calculated area radius

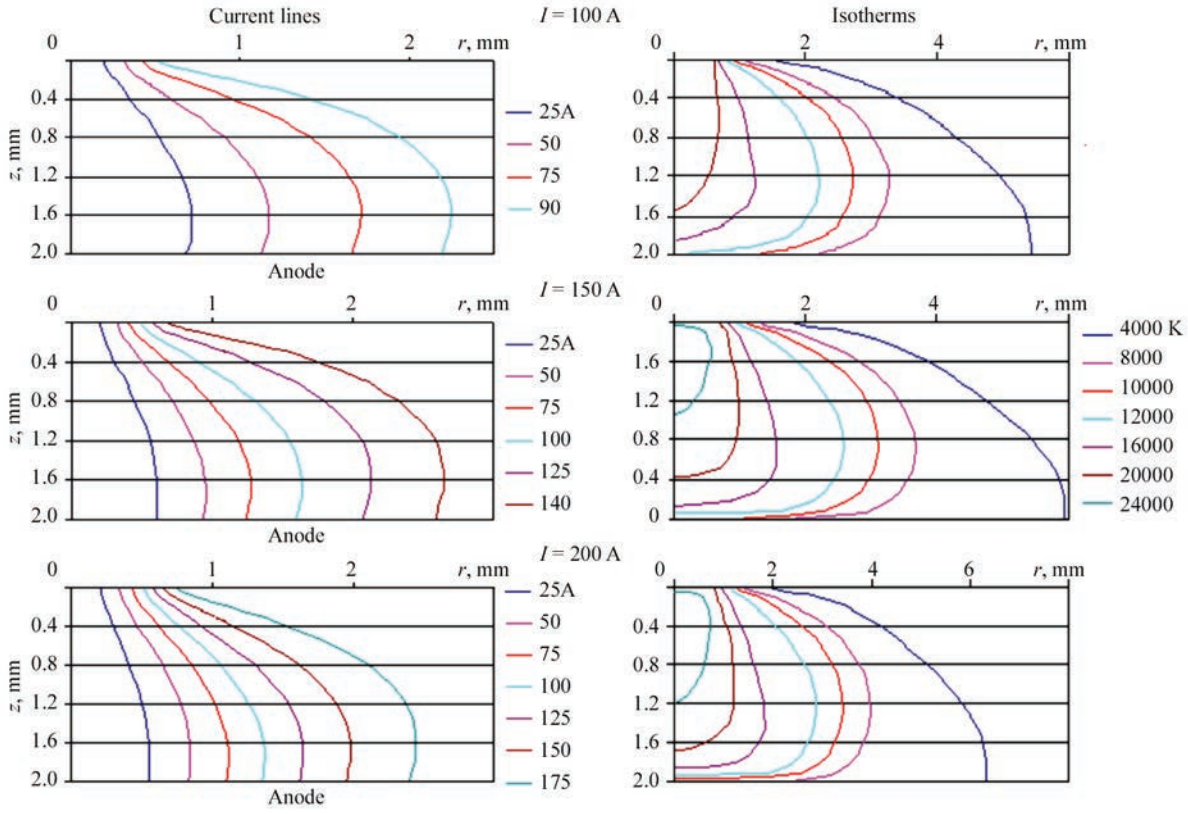

Figure 2. Current lines and isotherms of temperature field in the arc column

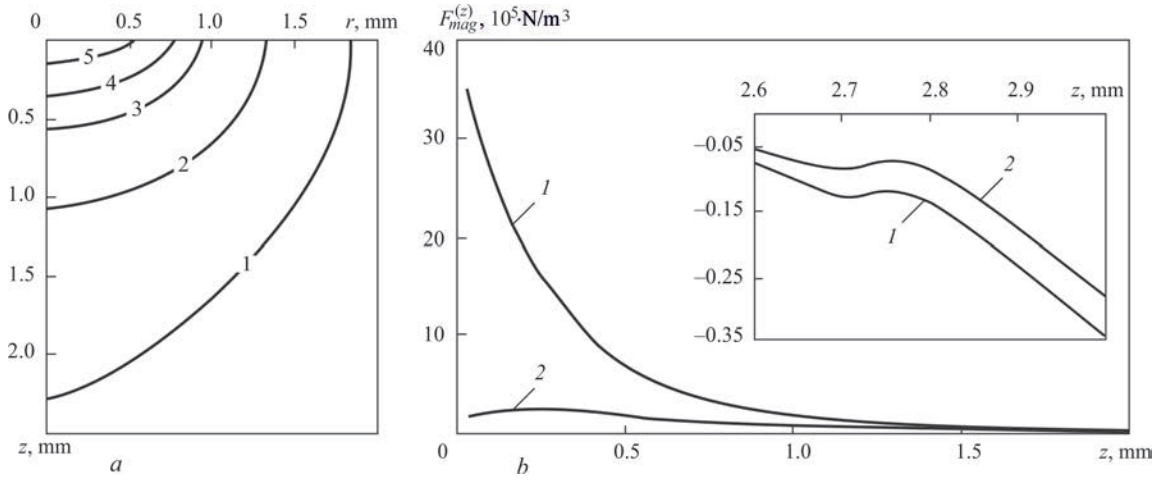

Figure 3. Force characteristics of electromagnetic field in arc column: *a* — magnetic pressure isobar field (*1* — P_{mag} = 100; *2* — 200; *3* — 400; *4* — 600; *5* — 1000 Pa); *b* — distribution of axial component of the magnetic force along the arc column length (*1* — on arc axis; *2* — at *r* = 1 mm)

$$F'_{rot}(r,z) = -\mu_0 \frac{I^2(r,z)}{4\pi^2 r^3}\vec{e}_r,$$

where {*r*, *z*} are the cylindrical coordinates (see Figure 1); $\vec{e}_r$ is the unit radius–vector; *I*(*r*, *z*) is the current flowing through a circle of radius *r* in the axial section *z* of the arc column; μ_0 is the universal magnetic constant.

This centrifugal force induces magnetic pressure in the current channel

$$P_{mag}(r,z) = -\int_r^\infty F_{rot}(r,z)dr,$$

the gradient of which can be treated as a certain force of magnetic nature $\vec{F}_{mag}$, exciting the movement of arc plasma from the region of high values of magnetic pressure towards its decrease.

Results of the conducted computational experiments are indicative of the fact that in the arc column regions with a higher current density, the compressive action of vortex force $\vec{F}_{rot}$ becomes stronger, and magnetic pressure rises, accordingly. Figure 3 illustrates the distribution of force characteristics of the electromagnetic field in the arc column 3 mm long at the current of 150 A. Magnetic pressure value is maximum in the axial zone of the near-cathode region of the arc column, and decreases quickly along the radius and along coordinate *z*, measured from the cathode (see Figure 3, *a*). In the considered case, the maximum value of magnetic pressure does not exceed 1000 Pa that is equal to less than 1 % of atmospheric pressure. However, a rapid change of magnetic pressure in the above region results in its gradient being quite significant. Thus, in the axial zone of near-cathode plasma the axial component of magnetic force $F_{mag}^{(z)}$ reaches the value of the order of $3 \cdot 10^6$ N/m^3 (see Figure 3, *b*).

Magnetic force localizing in the axial zone of near-cathode plasma initiates movement of arc plasma, mainly, in the direction from the cathode to the anode. In the middle part of the arc column the magnetic pressure gradient becomes negligibly small, and plasma movement continues by inertia. Near the anode surface, this gradient changes its sign (see insert in Figure 3, *b*), i.e. magnetic force turns out to be directed away from the anode to the cathode. In the conditions considered here, the force of inertia of the plasma flow in the near-anode region of the arc column is greater than $F_{mag}^{(z)}$. Therefore, the action of the latter is limited just by partial deceleration of the plasma flow, alongside its gas-dynamic deceleration near the anode surface. In nonconsumable electrode welding, the anode current density can be significantly increased through application of special technological means, such as, for instance, use of activating flux [17], arc exposure to focused CO_2-laser radiation [18]. In this case, the axial component of magnetic force near its surface, while remaining negative, rises in absolute value and at certain dimensions of the region of anode attachment of the arc, it remains capable of counteracting the force of inertia of the plasma flow. This can result in appearance of arc plasma movement towards the incoming plasma flow in near-anode plasma. Gas-dynamic interaction of these two flows is capable of creating two-vortex circulation of plasma in the arc column (see scenario 2 in work [16]).

Distribution of axial component of the vector of the velocity of plasma movement along the arc axis is given in Figure 4.

It is characteristic that at small values of arc current, the start of deceleration of the plasma flow is shifted closer to the cathode, whereas with current increase the deceleration region shifts towards the anode. Note also that with increase of arc length the

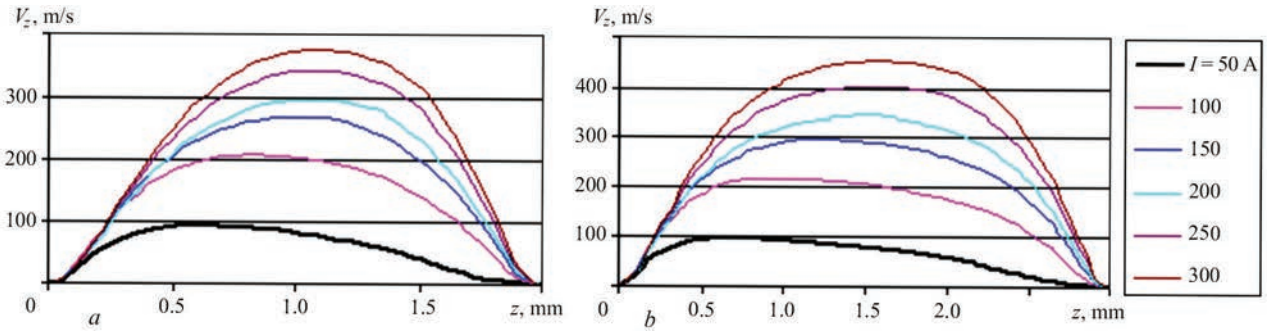

Figure 4. Distribution of axial component of the vector of plasma velocity along the arc axis: *a* — *L* = 2; *b* — *3* mm

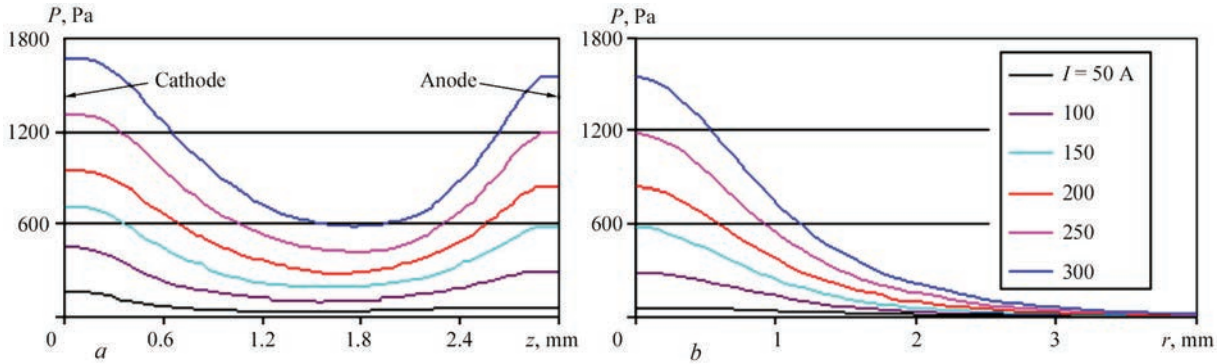

Figure 5. Total pressure of plasma in 3 mm long arc: *a* — on arc axis; *b* — on anode surface

velocity of plasma flow movement rises markedly, which is accounted for by increase of transverse dimensions of its column (see Figure 2) and lowering of its gas-dynamic resistance, accordingly.

Distributions of total pressure on the axis of 3 mm long arc and on the anode surface are shown in Figure 5. Pressure varies nonmonotonically along the arc axis (see Figure 5, *a*): near the cathode it is higher as a result of the compressive impact of vortex force $\vec{F}_{rot}$ (r, z) and high values of magnetic pressure, respectively (see Figure 3, *a*); in the center of arc column total pressure decreases as a result of radial unloading of the plasma flow and relatively small magnetic pressure, and near the anode the pressure rises again

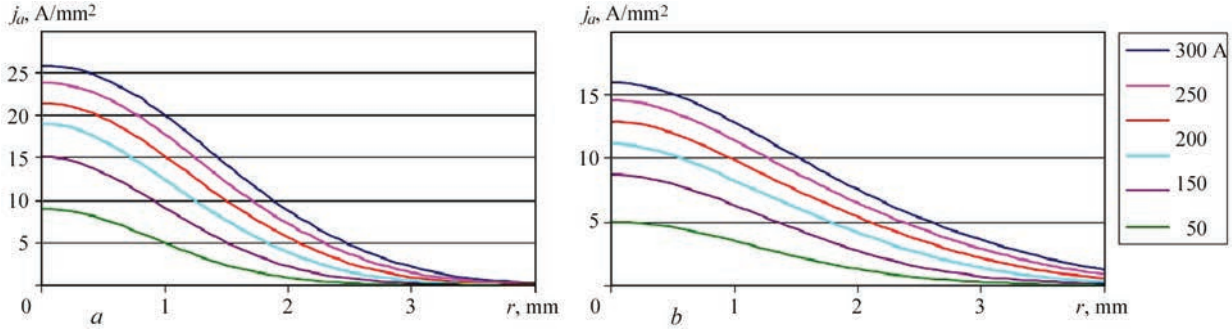

Figure 6. Distribution of arc current density on anode surface: *a* — *L* = 2; *b* — 3 mm

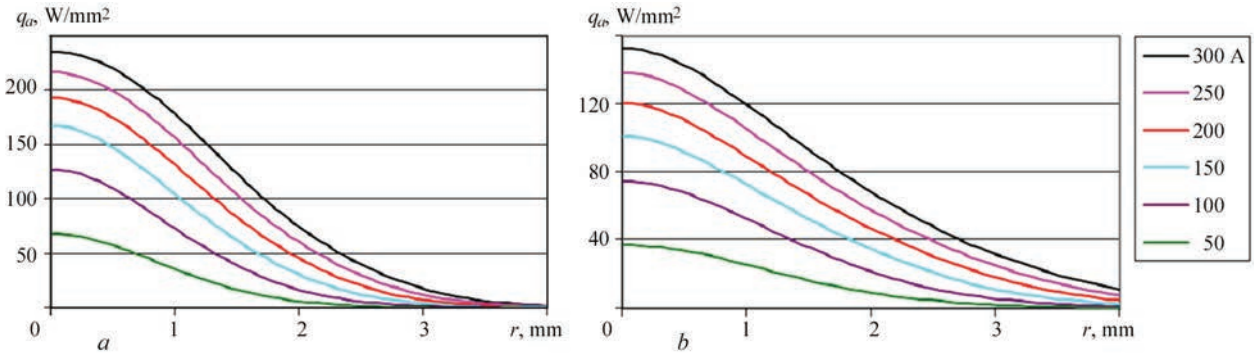

Figure 7. Distribution of heat flow applied by the arc to the anode: *a* — *L* = 2; *b* — 3 mm

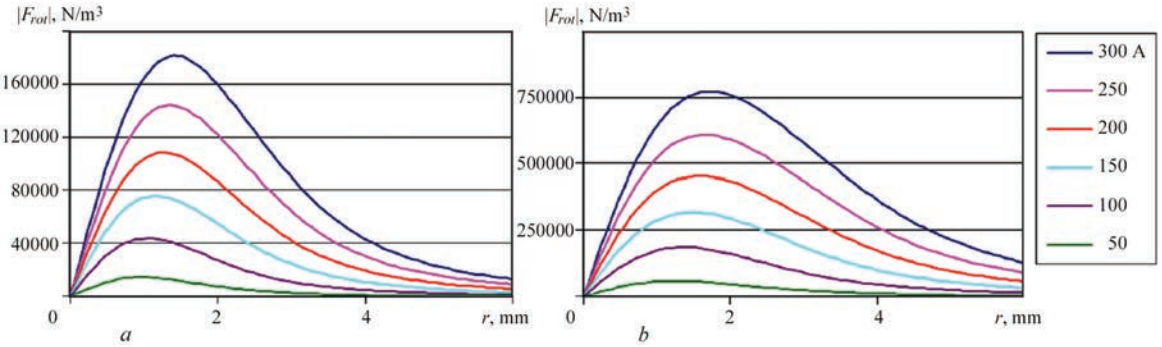

Figure 8. Distribution of vortex component of the Lorentz force along the anode surface: *a* — *L* = 2; *b* — 3 mm

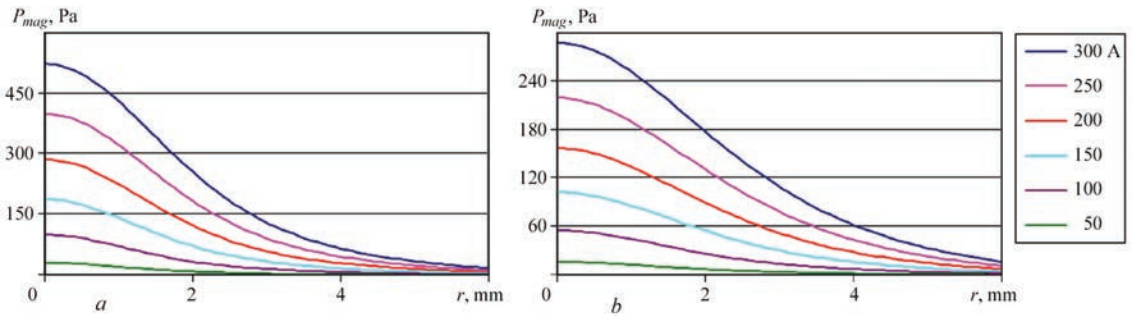

Figure 9. Distribution of magnetic pressure along anode surface: *a* — *L* = 2; *b* — 3 mm

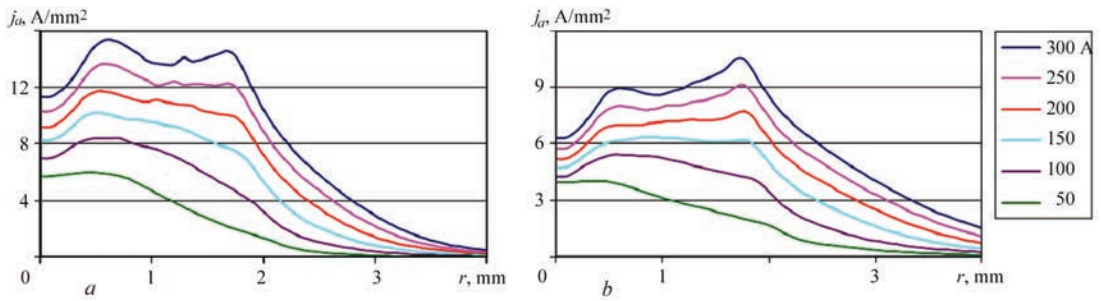

Figure 10. Distribution of arc current density over the surface of evaporating anode: *a* — *L* = 2; *b* — 3 mm

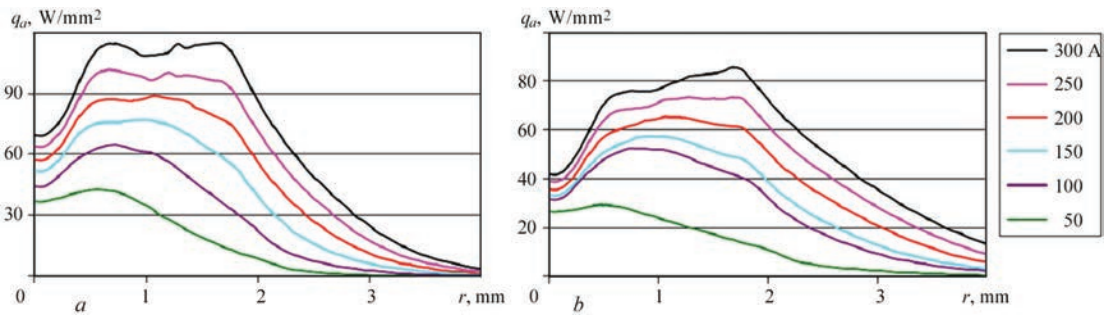

Figure 11. Distribution of heat flow brought by the arc to the evaporating anode: *a* — *L* = 2; *b* — 3 mm

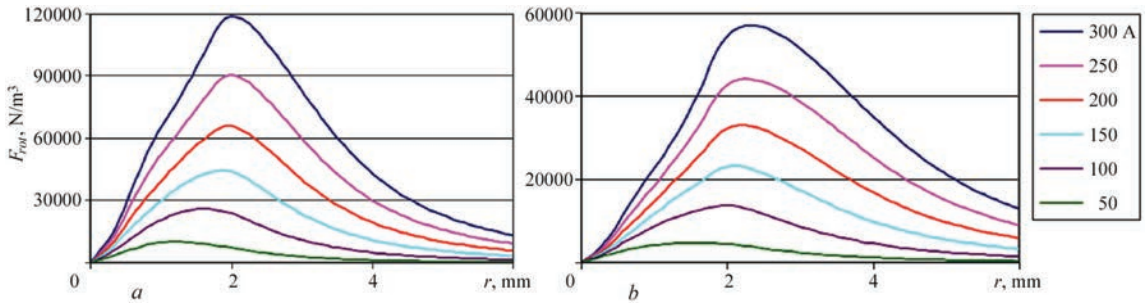

Figure 12. Distribution of vortex component of Lorentz force along the evaporating anode surface: *a* — *L* = 2; *b* — 3 mm

as a result of deceleration of the plasma flow on its surface. Note that the fields of pressure in 2 and 3 mm long arcs differ only slightly. As regards total pressure on the anode surface, it rises with increase of arc current (see Figure 5, *b*).

It should be emphasized that the given in Figure 5, *b* distribution of total pressure over the anode surface forms as a sum of magnetic pressure and gas-dynamic pressure of incoming plasma flow. Considering that the jump of magnetic pressure on «plasma–anode metal interface» is equal to zero, from the view point of deformation of the weld pool free surface just the gas-dynamic pressure is relevant, which is the result of deceleration of the plasma flow near the above surface.

Characteristics of the arc anode region. Let us consider the distributed characteristics of electric, thermal and force impact of arc plasma on the anode surface. Figures 6, 7 give the distributions of the density of electric current $j_a(r)$ and heat flow $q_a(r)$, brought by the arc to the anode, over the surface of water-cooled (nonevaporating) anode. As follows from calculated dependencies, shown in these Figures, the anode current density and specific heat flow to the anode decrease with increase of the arc length, that is in agreement with experimental data of work [19].

With shortening of the arc length, anode current contraction becomes higher: calculated values of anode current density on the axis of 2 mm long arc are more than 1.5 times higher compared to 3 mm arc (compare with Figure 6, *a*, *b*). The force impact of vortex component of Lorentz force $\vec{F}_{rot}$ increases accordingly, both on the weld pool surface, and in its volume, leading to intensification of gas-dynamic flow of the melt and higher penetrability of the arc [16]. Distributions of $|F_{rot}|$ over the anode surface for 2 and 3 mm long arcs are shown in Figure 8, and magnetic pressure distributions are presented in Figure 9.

An important factor, influencing the characteristics of arc column plasma and its interaction with the anode surface in nonconsumable electrode welding, is multicomponent nature of arc plasma, associated with metal evaporation from the weld pool surface. Figures 10–12 give the distributions of current density, heat flow and vortex component of the Lorentz force on the surface of an anode from low-carbon steel, evaporating in the diffusion mode, at model distribution of its temperature in the zone of anode attachment of the arc: $T_s(r) = (T_{s0} - T_\infty)\exp(-a^2r^2) + T_\infty$, where T_{s0} = 3050 K is the surface temperature on the arc axis; T_∞ = 500 K is the surface temperature at considerable distance from the axis, and the concentration ratio *a* is determined so that the radius of the molten zone on the surface of the steel anode was equal to 2.5 mm [20].

As follows from comparison of Figure 10 and Figure 6, the current density on the surface of the evaporating anode turns out to be considerably smaller than in the case of water-cooled anode, the most marked lowering of $j_a(r)$ being observed in the center of the region of anode attachment of the arc, where the local minimum of the above value is reached. Density of heat flow brought by the arc to the evaporating anode behaves in a similar way (compare Figure 11 and Figure 7). As regards reduction of the density of current and heat flow into the anode at increase of arc length (see Figures 6, 7), this tendency is preserved also for the evaporating anode (see Figure 10, *a*, *b* and Figure 11, *a*, *b*).

The noted lowering of current density on the anode surface, allowing for its material evaporation, results in the respective reduction of vortex component of Lorentz force $\vec{F}_{rot}$ on the weld pool surface (see Figures 8, 12), that leads to weakening of convective heat transfer in its volume, thus lowering the penetrability of an arc with evaporating anode.

Another factor, determining the characteristics of the electric, thermal and force impact of the arc on the anode surface, is the fact that the anode potential drop U_a, defined as the difference of anode surface potential φ_a and plasma potential on anode layer boundary φ_{pa}, is not constant in the region of anode attachment of the arc. In view of the high conductivity of metallic materials, the anode surface is practically equipotential, that is why the anode electric potential φ_a can be considered constant with good approximation. As regards value φ_{pa}, then, as its determining parameters (near-anode plasma temperature and anode current density) have nonuniform distributions along the anode surface (see Figure 2, *b*), the above value and, therefore, the anode potential drop also are nonuniform in the region of anode attachment of the arc [20].

As an illustration, Figure 13 gives the distributions of plasma potential along the boundary of anode layer with the column of the arc with refractory cathode and copper water-cooled anode, 2 and 3 mm long, in comparison with the respective distribution of near-anode plasma temperature. The large slope of $\varphi_a(r)$ dependence for 2 mm arc, compared to 3 mm arc at 100 A current (see Figure 13, *a*) is due to a similar nature of temperature curve change (see Figure 13, *b*).

As the anode layer boundary is isopotential, there exists a different from zero radial gradient of potential, and, accordingly, the current density vector has radial component j_r. Here, the greater the steepness of φ_{pa} radial change, the larger is the respective component of current density. This effect is illustrated in Figure 4,

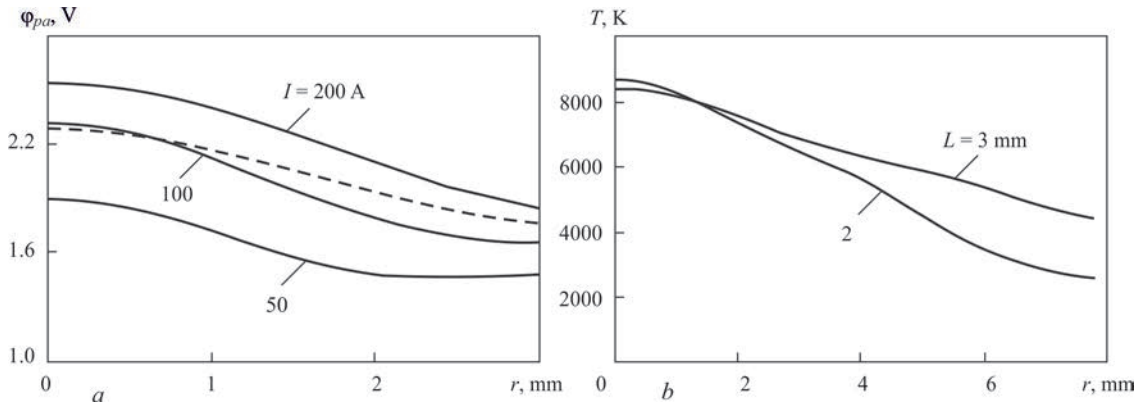

Figure 13. Distributions of plasma potential along the boundary of anode layer and arc column (*a*) at different values of current of 2 mm long arc (solid curves), and for 100 A arc of 3 mm length (dashed curve), as well as temperature distributions of near-anode plasma along the anode surface (*b*) for 100 A arc of 2 and 3 mm length (anode surface potential is taken to be constant and equal to zero)

which shows the change of j_r along the boundary of anode layer for 2 and 3 mm arcs at 100 A current. With j_r increase (for shorter arcs) the angle between the vector of anode current density and arc axis increases, that is indicative of a stronger contraction of the current channel in the direction to the anode and higher anode current density, respectively (see Figure 6).

In conclusion of this section, special attention should be paid to the fact that the anode potential drop $U_a = U_a = \varphi_a - \varphi_{pa}$ in the considered arcs is negative, that is in agreement with the known calculated and experimental data [8, 13, 21, 22].

Integral characteristics of the arc. An important integral characteristic, determining the electric and energy properties of the arc discharge, is its volt-ampere characteristic (VAC), which relates voltage across the arc gap U with arc current I. Figure 15 shows the results of approximation by the procedure, described in [23], of experimental data on VAC of an argon arc with a refractory cathode and copper water-cooled anode at different values of arc length: L = 1.5; 2, 3 mm. The volt-ampere characteristic of the arc can be associated with its watt-ampere characteristic, correlating arc power $P = IU$ with current I (see Figure 15, *b*).

Total arc voltage U is usually presented as sum $U = U_c + U_p + U_a$, where U_c is the cathode voltage drop; U_p is the arc column voltage; U_a is the anode drop [24]. Accordingly, the arc power can be presented in the following form $P = P_c + P_p + P_a$, where $P_c = U_c I$, $P_p = U_p I$ and $P_a = U_a I$ are the powers released in the cathode region, arc column and anode region, respectively. Since the anode drop is negative ($U_a < 0$), as was noted above, arc power P is smaller than the total power, released in the column and cathode region of the arc by value $|P_a|$, consumed for maintaining the anode layer. These, on the whole, correct relationships, require further refinement from the viewpoint of what should be understood by values U_c, U_p, U_a, allowing for the change of electric potential along the interfaces of the anode and cathode regions with the arc column.

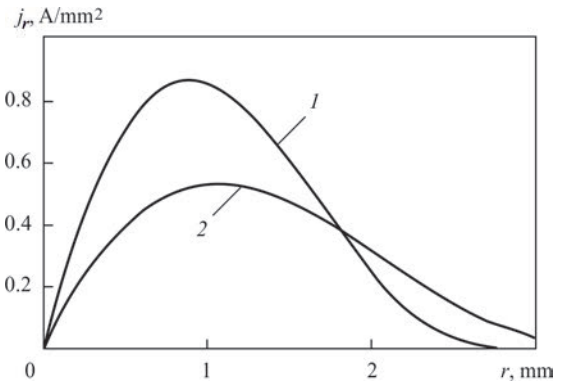

Figure 14. Distributions of radial component of current density vector along the anode surface: *1* — L = 2; *2* — 3 mm

In view of the high conductivity of anode and cathode metal, potentials φ_a and φ_c of their surfaces can be assumed to be practically constant. Therefore, total arc voltage can be determined as the difference of the respective potentials, i.e. $U = \varphi_a - \varphi_c$. Such a generally accepted definition of voltage in the form of the difference of potentials is not suitable for calculation of the cathode and anode drops, or arc column voltage. Therefore, another definition of the above values should be given, and so that integral Ohm and Joule–Lentz laws remained valid. With this purpose, we will introduce effective (averaged) values of potentials Φ_{pa} and Φ_{pc} on boundaries Γ_{pa} and Γ_{pc}, separating the anode and cathode regions from the arc column, as follows:

$$\Phi_{pa} = \frac{1}{I}\int\limits_{\Gamma_{pa}} \varphi j_n d\Gamma_{pa}; \Phi_{pc} = \frac{1}{I}\int\limits_{\Gamma_{pc}} \varphi j_n d\Gamma_{pc} \quad [20].$$

Then effective voltage drop across the arc column can be determined as the difference of effective values of the respective potentials, i.e. we can assume $\langle U_p \rangle = \Phi_{pa} - \Phi_{pc}$. Effective anode $\langle U_a \rangle = \varphi_a - \Phi_{pa}$ and cathode $\langle U_c \rangle = \Phi_{pc} - \varphi_c$ potential drops are determined similarly.

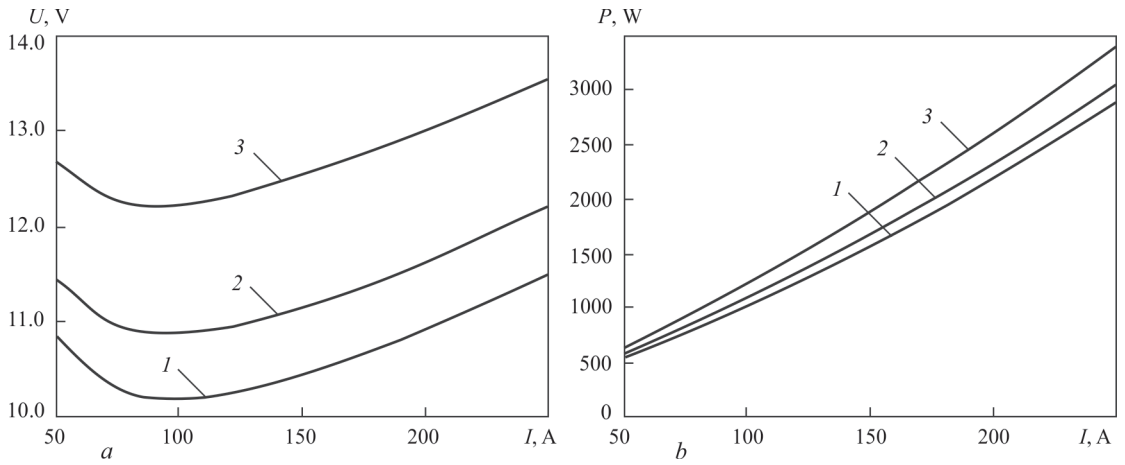

Figure 15. Volt- (*a*) and watt-ampere (*b*) characteristics of an argon arc with refractory cathode and copper water-cooled (nonevaporating anode): *1* — L = 1.5; *2* — 2; *3* — 3 mm

Figure 16 gives the scheme of distribution of electric potential φ and effective components of voltage in the arc gap introduced as showed above. Here, total arc voltage can be presented as a sum of respective effective components: $U = \langle U_c \rangle + \langle U_p \rangle + \langle U_a \rangle$, allowing for $\langle U_a \rangle < 0$. In terms of the introduced effective values of voltage drop in individual regions of the arc, the total balance of the respective powers can be written similarly: $P = \langle P_c \rangle + \langle P_p \rangle + \langle P_a \rangle$, where $\langle P_c \rangle = I\langle U_c \rangle$, $\langle P_p \rangle = I\langle U_p \rangle$, $\langle P_a \rangle = I\langle U_a \rangle$. Here, the integral Joule–Lenz law remains valid both for individual components of the arc discharge, and for the arc as a whole.

It does not seem possible to give a theoretical evaluation of effective value of cathode potential drop within the used model of the arc [14, 15], because of an approximate description of the cathode region. However, if the volt-ampere characteristic of the arc is known (see Figure 15, *a*), the effective cathode drop can be calculated from the following formula $\langle U_c \rangle = U - \langle U_p \rangle - \langle U_a \rangle$, using the calculated data on effective potential drops $\langle U_p \rangle$, $\langle U_a \rangle$, as well as experimentally measured arc voltage U.

Figure 17 gives the experimental and calculated dependencies of U, $\langle U_p \rangle$, $\langle U_a \rangle$ on current for an argon arc of 2 mm length, burning between the refractory cathode and copper water-cooled anode. The values of effective cathode potential drop, depending on arc current, calculated as shown above, are given in Figure 18. This figure also gives the results of experimental determination of the cathode drop [25]. Comparison of calculated and experimental data shows their correspondence with the accuracy not lower than 15 % that is indicative of quite acceptable adequacy of the mathematical model, used in this work.

Let us now turn to integral characteristic of the anode processes in considered arcs. As follows from Figure 17, *b*, the effective anode potential drop in the argon arc with refractory cathode and copper water-cooled anode, being negative, increases in absolute value with increase of arc current. Its length has practically no effect on $\langle U_a \rangle$. The role of anode potential drop in the total arc voltage is quite significant. In particular, at current of 200 A, the calculated value of effective anode drop for 3 mm long argon arc is 2.24 V, that is equal to about 17 % of arc voltage U = = 13 V (see curve *3* in Figure 15, *a*). Energy consumption for maintaining the anode layer and the total arc power P correlate likewise.

An important factor, affecting the anode potential drop in arcs with a refractory cathode, is anode material evaporation. Calculated dependencies of $\langle U_a \rangle$ on I for 2 mm long arcs with copper water-cooled anode and steel evaporating anode are given in Figure 19. As follows from the curves shown in this Figure, effective value of anode drop in an arc with an evaporating cathode, while remaining negative, turns out to be smaller by absolute value than the respective value for an arc with a copper water-cooled anode practically in the entire considered current range.

In the theory of thermal processes in welding, it is accepted to evaluate the total heat flow:

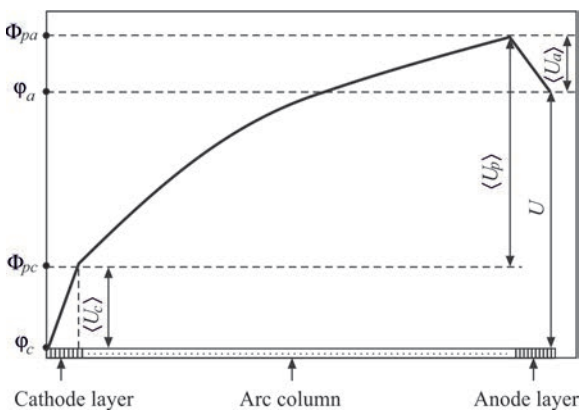

Figure 16. Scheme of electric potential distribution and effective components of arc voltage

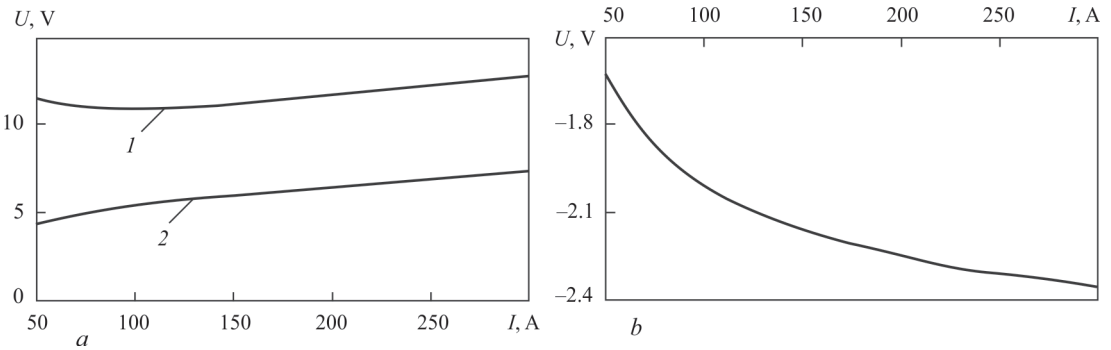

Figure 17. Voltage of 2 mm long arc and its components, depending on current: *a* — total arc pressure *U* (*1* — experiment); effective value of arc column voltage $\langle U_p \rangle$ (*2* — calculation); *b* — effective value of anode potential drop $\langle U_a \rangle$ (calculation)

$$Q_a = 2\pi \int_0^\infty r q_a(r) dr,$$

brought by the arc to the anode, proceeding from a simple formula $Q_2 = \eta P$, where η is the effective efficiency of the arc, determined experimentally. This expression is not universal, as value η at TIG welding depends on current and arc length, material being welded, shielding gas and other welding conditions. Therefore, determination of effective efficiency of the arc requires conducting the calorimetric measurements in each specific case that is unproductive. Instead of that, we can perform estimation of value Q_a, depending on current and length of the arc that will allow determination of respective η value, knowing its watt-ampere characteristic.

Let us first evaluate the effective radius of the current or heat spots of the arc (R_c, R_h, respectively) on the surface of a copper water-cooled anode, depending on arc current and length. By effective radius of the current or heat spot we mean the radius of a circle, within which 95 % of arc current *I* or, accordingly, total heat flow Q_a applied by the arc to the anode, are concentrated. Data given in Figure 20, show that in the entire considered range of currents $R_c \approx R_h$, and they increase practically linearly with *I* rise. In addition, as was anticipated, the dimensions of the zone of current and thermal impact of the arc on the anode surface become larger with increase of arc length.

Calculated dependencies of total heat power

$$Q_a = 2\pi \int_0^\infty r q_a(r) dr,$$

applied to the copper water-cooled anode on arc current and length, are given in Figure 21, from which it follows that value Q_a grows practically linearly with increase of arc current. As was already noted, specific heat flow $q_a(r)$ included into Q_a definition, decreases with increase of arc length (see Figure 7). Despite that, the total heat flow into the anode turns out to be even somewhat larger for a 3 mm arc than for 2 mm arc (see Figure 21). This feature of longer arcs is attributable, on the one hand, to increase of arc discharge power (arc voltage rises at the same current),

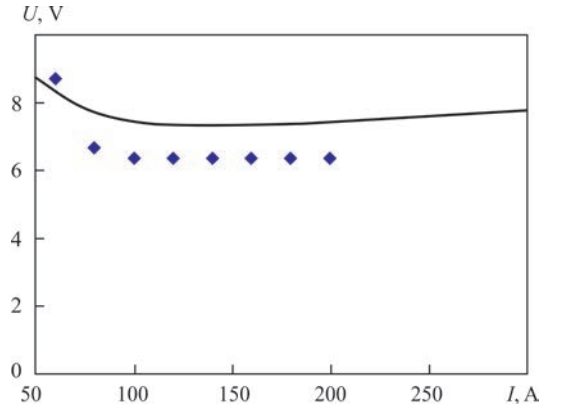

Figure 18. Effective cathode potential drop $\langle U_c \rangle$: solid curve — calculation; markers — experimental data [25]

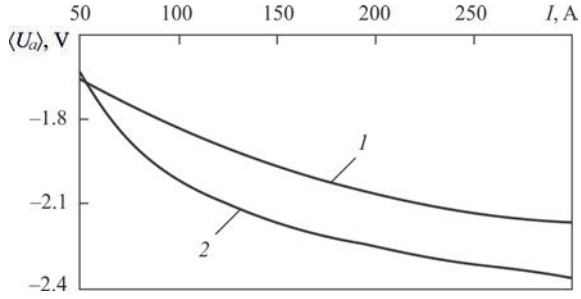

Figure 19. Dependencies of effective value of anode potential drop on current of an arc with steel evaporating anode (*1*) and copper water-cooled anode (*2*)

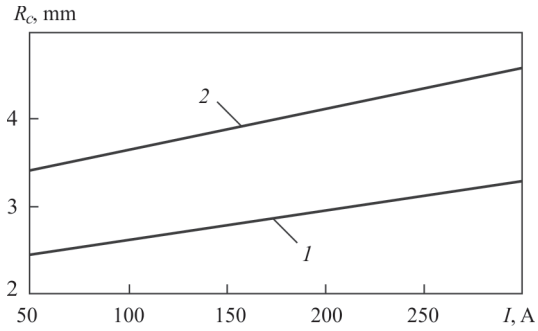

Figure 20. Dimensions of current and heat spots of the arc on anode surface: *1* — *L* = 2; *2* — 3 mm

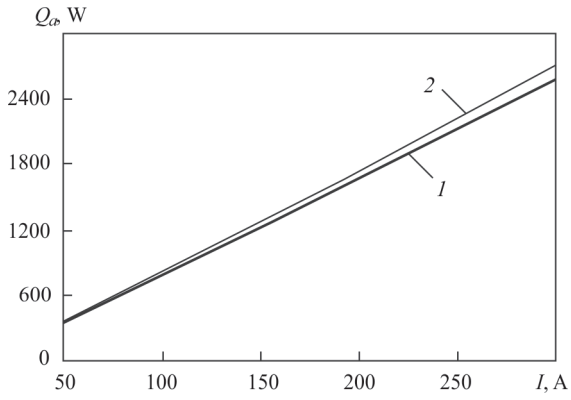

Figure 21. Total heat flow brought by the arc to the anode: *1* — L = 2; *2* — 3 mm

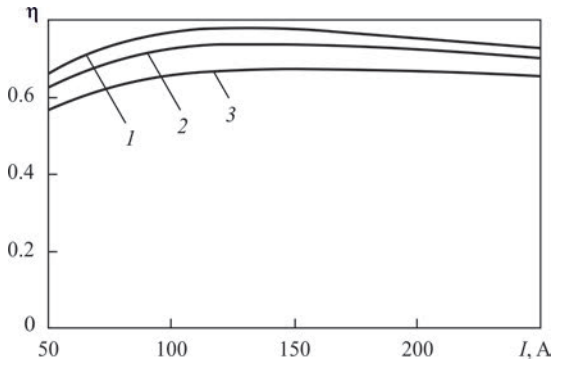

Figure 22. Dependencies of effective efficiency of an arc with copper water-cooled cathode on arc current and length: *1* — L = 1.5; *2* — 2; *3* — 3 mm

and, on the other hand, increase of the diameter of the zone of thermal impact of the arc on the anode surface (see Figure 20). As regards comparison of calculated values with those measured experimentally, according to the data of [26], the above-mentioned value is equal to 2.05 kW at I = 200 A, L = 3 mm, and differs from calculated value Q_a = 1.8 kW (see curve *2* in Figure 21) by not more than 15 %.

Data given in Figure 21, together with the experimental data on watt-ampere characteristic of the arc (see Figure 15, *b*) allow conducting calculated-experimental estimate of effective efficiency by formula η = Q_a/P. The thus calculated η values for arcs of different length, depending on current, are shown in Figure 22, and are indicative of the fact that the arc efficiency decreases wit increases of its length, and, in addition, in the considered current range η value has a maximum, which is in the interval from 130 up to 170 A.

In conclusion of this section it should be noted that the processes of heating and melting of the metal being welded (temperature field, weld pool shape and dimensions) are determined not only by Q_a or η value, but also depend on such arc impact characteristics, distributed over the surface of metal being welded, as specific heat flow into the anode and density of electric current on its surface. These characteristics have different effects on thermal state of the metal being welded: the first of them is responsible for conductive energy transfer (heat conduction mechanism), and the second determines the intensity of hydrodynamic flows, and convective heat transfer in the molten metal, accordingly.

Discussion and conclusions. Given in this work results of calculation of distributed and integral characteristics of free-burning argon arc with a refractory cathode and their dependencies on arc current and length are quite predictable in terms of quality. A new circumstance, which was revealed due to introduction of current lines into consideration, is the effect of constriction of the current channel in near-anode region, which is manifested in the entire considered range of arc currents and lengths. With increase of the density of electric current on the surface of the anode (metal being welded), the force impact of arc current on weld pool metal becomes stronger, that promotes an increase of the velocity of melt flowing into the pool bottom part, and, as a result, greater depth of penetration of the metal being welded. Thus, unlike the theory of thermal processes in welding, based on heat conductance mechanism of energy transfer, the law of distribution of the density of heat flow into the anode is not the only characteristic, determining the weld pool shape. Another, not less important factor, influencing the arc penetrability, is the law of distribution of current density on the surface of the metal being welded. At all other conditions being equal, we should try to reduce the size of current channel, and increase the density of electric current on anode surface, accordingly повысить проницаемость дуги с тугоплавким катодом. In this context, the arc length is not the only parameter, allowing control of anode current distribution. There are a number of techniques in the arsenal of welding science, which allow increasing the anode current density: use of activating fluxes, selection of special composition of shielding gas (gas mixture), arc exposure to focused laser radiation, high-frequency pulse modulation of welding current, etc. Application of these effects, activating the arc process, and of their synergic combinations is a promising direction for improvement of the nonconsumable electrode welding process.

1. Hsu, K.C., Etemadi, K., Pfender, E. (1983) Study of the free-burning high-intensity argon arc. *J. of Appl. Phys*., 54, **3**, 1293–1301.
2. Hsu, K.C., Pfender, E. (1983) Two-temperature modeling of the free-burning high-intensity arc. *Ibid.*, 54, **8**, 4359–4366.
3. Lowke, J.J., Morrow, R., Haidar, J. (1997) A simplified unified theory of arcs and their electrodes. *J. Phys. D: Appl. Phys*., **30**, 2033–2042.
4. Haidar, J. (1999) Non-equilibrium modeling of transferred arcs. *Ibid*, **32**, 263–272.

5. Sansonnets, L., Haidar, J., Lowke, J.J. (2000) Prediction of properties of free burning arcs including effects of ambipolar diffusion. *Ibid.*, **33**, 148–157.
6. Masquere, M., Freton, P., Gonzalez, J.J. (2007) Theoretical study in two dimensions of the energy transfer between an electric arc and an anode material. *Ibid.*, **40**, 432–446.
7. Tanaka, M., Yamamoto, K., Tashiro, S. et al. (2008) Metal vapour behaviour in gas tungsten arc thermal plasma during welding. *Welding in the World*, 52(**11–12**), 82–88.
8. Dinulescu, H.A., Pfender, E. (1980) Analysis of the anode boundary layer of high intensity arcs. *J. of Appl. Phys*, **51**, 3149–3157.
9. Dyuzhev, G.A., Nemchinsky, V.A., Shkolnik, S.M. et al. (1983) Anode processes in high-current arc discharge. *Khimiya Plazmy*, **10**, 169–209 [in Russian].
10. Nazarenko, I.P., Panevin, I.G. (1989) Analysis of the near-anode processes character in argon arc discharge of high pressure. *Contrib. Plasma Phys*., **29**, 251–261.
11. Jenista, J., Heberlein, J.V.R., Pfender, E. (1997) Numerical model of the anode region of high-current electric arcs. *IEEE Trans. on Plasma Science*, **25**, 883–890.
12. Amakawa, T., Jenista, J., Heberlein, J. et al. (1998) Anode-boundary-layer behavior in a transferred, high intensity arc. *J. Phys. D: Appl. Phys*., **31**, 2826–2834.
13. Tanaka, M., Ushio, M., Wu, C.S. (1999) One-dimensional analysis of the anode boundary layer in free-burning argon arcs. *Ibid.*, **32**, 605–611.
14. Krivtsun, I.V., Demchenko, V.F., Krikent, I.V. (2010) Model of the processes of heat, mass and charge transfer in the anode region and column of the welding arc with refractory cathode. *The Paton Welding J.*, **6**, 2–9.
15. Krikent, I.V., Krivtsun, I.V., Demchenko, V.F. (2014) Simulation of electric arc with refractory cathode and evaporating anode. *Ibid.*, **9**, 17–24.
16. Demchenko, V.F., Krivtsun, I.V., Krikent, I.V. et al. (2017) Force interaction of arc current with self magnetic field. *Ibid.*,**3**, 15–24.
17. Yushchenko, K.A., Kovalenko, D.V., Krivtsun, I.V. et al. (2009) Experimental studies and mathematical modeling of penetration in TIG and A-TIG stationary arc welding of stainless steel. *Welding in the World*, 53(**9–10**), 253–263.
18. Krivtsun, I.V., Krikent, I.V., Demchenko, V.F. et al. (2015) Interaction of CO_2-laser beam with electric arc plasma in hybrid (laser-arc) welding. *The Paton Welding J.*, **3–4**, 6–15.
19. Yushchenko, K.A., Kovalenko, D.V., Kovalenko, I.V. (2005) Peculiarities of A-TIG welding of stainless steel. In: *Proc. of the 7th Int. Conf. on Trends in Welding Research — Pine Mountain, Georgia, USA*, 367–376.
20. Krivtsun, I., Demchenko, V., Krikent, I. et al. (2015) Distributed and integrated characteristics of the near-anode plasma of the welding arc in TIG and hybrid (TIG + CO_2-laser) welding. In: *Mathematical Modelling of Weld Phenomena 11 — Techn. Universität Graz, Austria*, 837–874.
21. Tanaka, M., Ushio, M. (1999) Observations of the anode boundary layer in free-burning arcs. *J. Phys. D: Appl. Phys*., **32**, 906–912.
22. Sanders, N.A., Pfender, E. (1984) Measurement of anode falls and anode heat transfer in atmospheric pressure high intensity arcs. *J. of Appl. Phys*., **55**, 714–722.
23. Sydorets, V.N., Krivtsun, I.V., Demchenko, V.F. et al. (2016) Calculation and experimental research of static and dynamic volt-ampere characteristics of argon arc with refractory cathode. *The Paton Welding J.*, **2**, 2–8.
24. Lancaster, J.F. (1986) *The physics of welding*. 2nd Ed. Pergamon Press.
25. Uhrlandt, D., Baeva, M., Kozakov, R. et al. (2013) Cathode fall voltage of TIG arcs from a non-equilibrium arc model. In: *IIW Essen, 2013, Group 212 – Physics of Welding*.
26. Nestor, O.H. (1962) Heat intensity and current density distributions at the anode of high current, inert gas arcs. *J. of Appl. Phys*., 33(**5**), 1638–1648.

Received 15.03.2019